Topology optimization for microwave control with reconfigurable intelligent metasurfaces in complex media

Theodosios D. Karamanos,* Mathias Fink, and Fabrice Lemoult
Institut Langevin, ESPCI Paris, Université PSL, CNRS, 75005 Paris, France

(Received 7 November 2023; revised 12 February 2024; accepted 18 March 2024; published 11 April 2024)

Reconfigurable intelligent metasurfaces have been proposed as an efficient solution for improving wireless telecommunication systems in multiple-scattering or reverberating media. Concurrently, topology optimization has been successfully used as an inverse-design technique in many fields, and particularly in electromagnetics. In this work, we apply a gradient-based topology optimization for tuning the binary elements of a metasurface for a focusing goal in a complex environment. First, the metasurface unit cells are approximated as point sources and, then, the optimization problem is formulated. Afterwards, the proposed method is applied to find the optimal parameter sets for three distinct environments of increasing complexity, and the resulting focus for each case is demonstrated via numerical simulations. The combination of a reverberating cavity and a metasurface inside the latter is very powerful since everything can be solved analytically for focusing outside the cavity.

DOI: 10.1103/PhysRevApplied.21.044022

I. INTRODUCTION

Wireless telecommunications have experienced rapid growth in recent decades, approaching a threshold where the presence of multiple paths degrades signal quality. Over the years, the idea of smart electromagnetic environments has emerged, foreseeing a fully programmable wave propagation to harness this complexity and achieve optimized transmission of both information and power and efficient electromagnetic wave shaping [1–3]. Reconfigurable intelligent metasurfaces (RISs) have emerged as a promising technology in this direction, with applications in fields ranging from efficient outdoor and indoor telecommunication and electromagnetic compatibility to imaging systems and quantum electrodynamics [4–6]. Research on RISs has focused on various contemporary topics, including improved wireless communications [7–9], indoor and cavity electromagnetic field shaping [10–13], and metamaterial imaging [14–16]. In principle, RISs are 2D arrays consisting of subwavelength tunable elements—namely, their electromagnetic response can be changed. Specifically, the unit cells of a RIS can be individually modified to scatter the incident field by, for example, addition of a phase. In the optical spectrum, this can be achieved by use of spatial light modulators (SLMs) as metasurface elements [17,18]. SLMs often consist of liquid-crystal cells that introduce a phase shift on the light they reflect (or that passes through them). The equivalent of SLMs in the microwave regime is spatial microwave modulators (SMMs) [10,19]. In the aforementioned designs, an SMM consists of a rectangular static patch, as a main reflector, and a strip, as a parasitic resonator, which is binary tunable with the help of an embedded p-i-n diode. In particular, by controlling the bias of the diode, one can achieve a binary pixel in microwaves: it re-emits the incident wave with a 0 phase shift or a π phase shift, i.e., acting as a perfect electric or magnetic conductor. SMMs provide an excellent, two-state unit cell for reconfigurable metasurfaces for microwaves, although various other setups exist that could provide efficient alternatives [20–22]. Another important theme in the research on RISs is their theoretical modeling, which could lead to efficient design and optimization. In contrast to common metasurface models [23,24], the unit cells in RISs are not identical, and thus the usual models must be modified. Although circuit models are occasionally used for the study of RISs [25], the use of microscopic models can increase the accuracy of the analysis, as well as provide greater understanding of the underlying physical problems [26–28]. Nevertheless, the lack or limited inclusion of mutual interaction between the unit-cells of the RIS or the inclusion of the coupling effects only on the phase of the scattered waves, may lead to inaccuracies and inefficient designs.

Because of the dynamic nature of communication systems or ever-changing goals "smarter," more-efficient, and faster methods are required for the reconfiguration of the tunable elements in comparison with "brute-force" methods, which are currently used in RISs [10,11]. As a more-efficient alternative, topology optimization is a

*Corresponding author: theodosios.karamanos@espci.fr

promising tool for such applications [29–32]. Originating from mechanical problems [33], this density-based inverse-design technique results in efficient devices for several purposes in electromagnetics, and, most notably, in photonics [29,31,34]. In this specific field, topology optimization has attracted considerable interest during the past few years, with examples including dielectric multiplexers [35,36], metalenses [37,38], and integrated photonic devices [39,40]. A particular characteristic of topology optimization is that it is a gradient-based optimization technique, where the gradient is, usually, acquired efficiently and swiftly by the adjoint method [29,30]. The gradient-based family of algorithms is generally faster than derivative-free methods (e.g., genetic algorithms or particle-swarm optimization) when a very large number of variables is involved [30]. Specifically, the non-gradient-based methods require more computational time and resources for convergence, and this problem becomes worse for a much-larger number of design variables [41, 42]. It has also been reported that sometimes gradient-based methods achieve a better local minimum or maximum [3,4,30,43]. In Ref. [30] an indicative comparison between topology optimization (gradient based) and a genetic algorithm is performed for inverse design in photonics, with the former outperforming the latter in terms of computational-resource demand. Hence, topology optimization as an inverse-design technique allows for a point-by-point material density variation in the structure under study, while it has demonstrated that it can produce optimized solutions for problems with hundreds of thousands of variables or more [29,32,38]. These features of topology optimization are very promising for potential applications in RISs, where thousands of tunable elements may need to be reconfigured quickly to achieve predetermined, yet changing, goals.

In this work, we develop a topology-optimization technique to be used for binary reconfigurable intelligent metasurfaces [10,19] when placed in complex media. Herein, we define this term to describe media where multiple reflections or scattering exists. Examples of such media include rooms with furniture, metallic cavities, or spaces with many scatterers with dimensions smaller than the wavelength. Our framework is based on a combination of the existing gradient-based topology-optimization techniques, with the use of the adjoint method, and the modeling of electromagnetic problems with Green's functions. First, we theoretically formulate the electromagnetic problem in two dimensions by assuming that the reconfigurable elements of the metasurface are two-state elements, i.e., a 0 phase shift or a π phase shift, and that they can be equivalently represented as point scatterers. Moreover, the optimization problem is formulated with the goal of maximizing the intensity at a given focus point via a certain binary phase set of the metasurface elements. Then, the adjoint method is used to ensure the fast computing of the gradients of the objective function. Finally, the optimization problem is reformulated using the 2D Green's functions for the representation of the interactions between the elements of the metasurface, the focus, and the source, ensuring an even-faster overall optimization process. Afterwards, we apply the theoretical formulation developed to focusing problems in three different environments of increasing complexity. We examine the efficiency of the resulting focus after the application of the topology-optimization scheme using different options for the interactions between the unit cells of the metasurface, while the possibility of analytical calculation or numerical extraction of the 2D Green's function values is explored for each complex medium under study. Notably we show that placing the source and the metasurface in a partially open cavity is a promising configuration since everything can be solved analytically.

II. THEORETICAL FORMULATION

A. Problem model

We first model the problem of using a reconfigurable metasurface in a complex environment, as depicted in Fig. 1, in a generalized fashion for 3D and 2D setups. Examples of complex media include highly reflecting environments [44], such as leaky closed cavities, an urban landscape, an office or domestic room with furniture, and multiple-scattering environments, such as an assortment of dielectric or metallic scatterers. Despite the different examples mentioned, the technique developed should be applicable to all types of scattering, from the case of clusters of small particles with dimensions smaller than the operating wavelength to the case of large geometric obstacles, such as metallic walls. The goal of the overall setup is electromagnetic focusing at a given point F of the energy coming from one or several emitters with the help of a tunable metasurface. Without loss of generality, we assume here that the system is excited only by a single point current source $\mathbf{J}_S$ at the point S (Fig. 1). The reconfigurable metasurface consists of N subwavelength elements

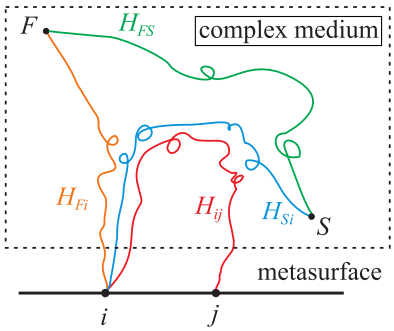

FIG. 1. The generalized 2D focusing problem in a complex medium and in the presence of a reconfigurable metasurface.

positioned on a lattice with unit-cell dimension $d < \lambda/2$. Moreover, the metasurface is considered to be made of elements that totally reflect the incident wave (whatever the angle) but the phase ϕ of reflection can be tuned from 0 to π. These two-state unit cells are ideal versions of a common theme with current technology for reconfigurable metasurfaces [10]. Mathematically, the reflectivity of pixel i can be expressed as $R_i = e^{-i\phi_i}$, with $\phi_i \in \{0, \pi\}$.

In that context, we decide to model the metasurface elements as current point sources at the center of the unit cells. We assume that the metasurface elements are much smaller than the operating wavelength, or $d \ll \lambda$, with d being the largest dimension of the scatterer. Therefore, we work in the Rayleigh-scattering regime. To model the desired reflectivity, the electric field re-emitted by a pointlike pixel i corresponds to $\mathbf{b}_i = R_i \mathbf{E}_i^{\text{loc}} = R_i(-i\omega\mu_0 \mathbf{J}_i)$, where $\mathbf{E}_i^{\text{loc}}$ is the local field at the element position to be retrieved and $\mathbf{J}_i$ is the equivalent current source. This approximation is valid as long as the dimensions of the scatterers are much smaller than the operational wavelength so that we work in the far field or the radiation zone [45]. Both R_i and $\mathbf{E}_i^{\text{loc}}$ depend on ϕ_i. Overall, the electromagnetic problem of a metasurface in a complex medium can be expressed with use of the Helmholtz equation as

$$\left(\nabla^2 + \frac{\omega^2}{c^2(\mathbf{r})}\right)\mathbf{E} = \mathbf{b}_s \delta(\mathbf{r} - \mathbf{r}_S) + \sum_{i=1}^{N} \mathbf{b}_i(\phi_i)\delta(\mathbf{r} - \mathbf{r}_i), \tag{1}$$

with $\mathbf{b}_s = -i\omega\mu_0 \mathbf{J}_S$ corresponding to the electric field generated by the source at the point S. The complex medium in Fig. 1 is nonhomogeneous, and thus the wave velocity in Eq. (1) is a function of the spatial position.

The optimization problem, in this case, consists in finding which binary phase configuration of the N elements will result in the largest intensity at the target point F (Fig. 1). It corresponds to maximizing the figure of merit $M = \|\mathbf{E}_F\|^2$. To efficiently and rapidly find all the phases ϕ_i that will maximize the figure of merit, we use the topology-optimization method for inverse design.

B. Topology optimization and adjoint method

In general, for structural, as well as electromagnetic topology optimization, a density-based material parametrization is used [30]. The material is represented by the continuous design field $p_i \in [0, 1]$, which maps the material distribution for each pixel i of the design domain. Therefore, the electromagnetic optimization problem is formulated with the use of Eq. (1) as

$$\max_{\mathbf{p}} \quad M = \|\mathbf{E}_F(p_i)\|^2$$

$$\text{subject to } \left(\nabla^2 + \frac{\omega^2}{c^2(\mathbf{r})}\right)\mathbf{E} = \mathbf{b}_s \delta(\mathbf{r} - \mathbf{r}_S) + \sum_{i=1}^{N} \mathbf{b}_i(p_i)\delta(\mathbf{r} - \mathbf{r}_i), \tag{2}$$

$$\text{with } 0 \le p_i \le 1, \quad i = \{1, 2, \ldots, N\}.$$

For the case of the tunable metasurface, the "material" is, herein, the phase shift induced by the pixel of the metasurface. However, since only two states are allowed, i.e., 0 or π, a binarization scheme needs to be applied on the variables p_i. Additionally, the gradient-based optimization algorithms, as a rule, require continuous and derivable functions, and thus step functions cannot be used as a filter. Therefore, we apply a *smoothed Heaviside function*:

$$\tilde{p}_i(p_i) = \frac{\tanh\left(\frac{\beta}{2}\right) + \tanh\left(\frac{p_i - \beta}{2}\right)}{\tanh\left(\frac{\beta}{2}\right) + \tanh\left(\frac{1-\beta}{2}\right)}, \quad \beta > 1, \tag{3}$$

where β is a threshold value. After binarization, a *linear interpolation* is applied, resulting in the phase of element i as

$$\phi_i(\tilde{p}_i) = \pi\tilde{p}_i - i\alpha\tilde{p}_i(1 - \tilde{p}_i). \tag{4}$$

Here α has the role of a second binarization scheme; it controls the nonphysical imaginary term that introduces an attenuation for all intermediate values between 0 and π [30,32]. Finally, to ensure an almost-perfect binary result for the phase values, we impose a continuation scheme by gradually increasing β, with a ratio β_{inc} for each individual run of the optimization algorithm. The iterations and, eventually, the whole optimization process stop when the *gray indicator* [40] is almost zero, or

$$\gamma = \frac{1}{N}\sum_{i=0}^{N} 4p_i(1 - p_i) \approx 0. \tag{5}$$

In this way, the resulting vector $\mathbf{p}$ is almost always of value 0 or 1. As an initial set of values, we use $p_i = 0.5$ for all i. The values of α, β, and β_{inc} are problem dependent, and a trial-and-error process is required to identify the best ones. Generally, low values of α, β, and β_{inc} could provide better focusing results at the cost of longer optimization-algorithm running times, effectively a trade-off process.

Afterwards, we use a gradient-based algorithm to solve the topology-optimization problem described above. This specific family of techniques uses the gradients, or sensitivities, $dM/d\mathbf{p}$. One could approximate the gradients via finite differences, but this process would involve solving or simulating the problem described by Eq. (2) for

every combination of the design variables p_i, leading to too-long computational times. Therefore, in this work, we use the more-commonly-used *adjoint sensitivity analysis* or, simply, the *adjoint method* [29,30,46,47]. The strategy requires the solving of only two distinct problems to compute all the required gradients. First, the solution of the so-called direct problem gives the field $\mathbf{E}_F$, and thus its intensity, at the focusing point F when a point current source is placed at S. Second, an adjoint problem is solved where F becomes the source with an amplitude given by $\mathrm{d}M/\mathrm{d}\mathbf{E}|_{\mathrm{F},\mathbf{p}} = \mathrm{Re}\{E_F(\mathbf{p})\} - \mathrm{i}\,\mathrm{Im}\{E_F(\mathbf{p})\}$ [48]. In particular, it permits one to evaluate the adjoint solution $\mathbf{E}_{\mathrm{adj}}$, which corresponds to the electric field values at the N metasurface elements. Hence, the gradients are obtained as [49]

$$\frac{\mathrm{d}M}{\mathrm{d}\mathbf{p}} = 2\mathrm{Re}\left\{\mathbf{E}_{\mathrm{adj}}\cdot\frac{\partial\mathbf{b}}{\partial\boldsymbol{\Phi}}\frac{\partial\boldsymbol{\Phi}}{\partial\tilde{\mathbf{p}}}\frac{\partial\tilde{\mathbf{p}}}{\partial\mathbf{p}}\right\},$$
$$\text{with}\quad\left(\nabla^2+\frac{\omega^2}{c^2(\mathbf{r})}\right)\mathbf{E}_{\mathrm{adj}} = \left.\frac{\mathrm{d}M}{\mathrm{d}\mathbf{E}}\right|_{F,\mathbf{p}}\delta(\mathbf{r}-\mathbf{r}_F). \tag{6}$$

After the required derivative $\mathrm{d}M/\mathrm{d}\mathbf{p}$ is obtained via the adjoint method, it is inserted into the function `fmincon`, which performs nonlinear constrained optimization and is included in MATLAB 2021b [50]. More specifically, from `fmincon`, we use the gradient-based optimization algorithm `sqp`, i.e., *sequential quadratic programming* [51]. This method is similar to the Newton-Raphson method [52], and it is used herein for constrained optimization. The Jacobian and Hessian matrices required for this algorithm can be retrieved numerically; however, to greatly increase the speed and the accuracy of the whole process, we generally seek to quickly retrieve the gradient via the adjoint method. Nevertheless, it should be noted that the focus of this work is specifically the rapid retrieval of the gradient of the objective function, and the reader could alternatively use a different gradient-based optimizer.

In the presented problem of a metasurface in a complex medium, $\mathbf{E}_{\mathrm{adj}}$ can be acquired, at least through numerical simulations, via two steps, a direct calculation and an adjoint one, while the terms $\partial\boldsymbol{\Phi}/\partial\tilde{\mathbf{p}}$ and $\partial\tilde{\mathbf{p}}/\partial\mathbf{p}$ are calculated analytically [49]. The term $\partial\mathbf{b}/\partial\boldsymbol{\Phi}$ is not as easily retrievable as the other terms via the model introduced in Eq. (1), due to the complex interaction between the elements of the metasurface through the complex medium. However, if one assumes that the elements do not interact with each other and that the local fields on the metasurface pixels depend only on the source and the medium, i.e., they do not depend on the phases of the individual elements, then $\partial b_i/\partial\phi_i = -ie^{-\mathrm{i}\phi_i}\mathbf{E}_i^{\mathrm{loc}}$. Afterwards, the local fields at the centers of the unit cells can be calculated during the direct simulation. This approximation is quite common in reconfigurable-metasurface applications and is known to provide adequate results. Nevertheless, the omission of the dependence of the field due to the other elements introduces inaccuracies and inefficiencies, which become larger when reconfigurable metasurfaces are placed in media apart from free space. Therefore, to alleviate these issues, in this work, we introduce a rigorous Green's function model, which leads to accurate calculations and potentially shorter optimization times.

C. Green's function formulation

The gradient in Eq. (6) can be retrieved through the calculation of $\mathbf{E}_F$. This can be achieved with the use of Green's functions [53]. To demonstrate this approach, we, at this point of the analysis and without loss of generality, transform the general 3D electromagnetic problem in Eq. (1) to two dimensions. To do so, we assume that the source at the point S is an out-of-plane line current (or towards the z axis for an x-y plane), $\mathbf{J}_S = I_S\hat{\mathbf{z}}$, while the equivalent sources at the unit-cell centers are similarly induced out-of-plane line currents, $\mathbf{J}_i = I_i\hat{\mathbf{z}}$. Moreover, all materials involved are assumed to be invariant in the out-of-plane direction. Therefore, all electric fields involved in this 2D problem have only a $\hat{\mathbf{z}}$ component. At this point, we use the Green's function $H_{\boldsymbol{\rho}\boldsymbol{\rho}'}$ as the electric field value E_z measured at coordinate $\boldsymbol{\rho}$ when a point source is situated at location $\boldsymbol{\rho}'$ (see Appendix A for free-space solutions). The positions $\boldsymbol{\rho}$ and $\boldsymbol{\rho}'$ can be replaced by the positions of the source at the point S, the focal spot F, or the pixel elements i, as shown in Fig. 1. Since the Helmholtz equation is reciprocal, even in an inhomogeneous environment, it holds that $H_{\boldsymbol{\rho}\boldsymbol{\rho}'} = H_{\boldsymbol{\rho}'\boldsymbol{\rho}}$.

With the help of these Green's functions, we can fully calculate E_F. In a matrix form, it is expressed as

$$E_{\mathrm{F}} = H_{FS}b_s + \mathbf{H}_F^{\mathrm{T}}\mathbf{b}, \tag{7}$$

where $\mathbf{H}_F^{\mathrm{T}} = [H_{F1}H_{F2},\ldots,H_{FN}]$ contains the Green's function values between the focusing point F and the metasurface elements and $\mathbf{H}_S^{\mathrm{T}} = [H_{S1}H_{S2},\ldots,H_{SN}]$ between the source point S and the metasurface elements.

To take into account the multiple interactions between the pixels of the metasurface, we need to rewrite the field on the pixels as

$$\mathbf{b} = [R]\left\{\sum_{n=0}^{+\infty}([H][R])^n\right\}\mathbf{H}_S b_s. \tag{8}$$

The square matrix $[H]$ contains the interelement coupling, that is to say the Green's functions H_{ij}, and $[R] = \mathrm{diag}\{R_1R_2,\ldots,R_N\}$ stands for the reflection coefficients of each metasurface pixel. The number $n \in \mathbb{N}$ in Eq. (8) refers to the number of reflections between the environment and

the metasurface that are taken into account for the calculation. If the problem involves a low-reflecting medium, e.g., a leaky room with a few objects inside [10], then no reflection or a single reflection ($n = 0$ or $n = 1$) may be a good approximation. For the general case of infinite reflections, the power series involves square matrices and convergence always holds for passive systems. Therefore, the magic of this matrix formulation is that one can readily write the final solution of the multiply scattering series as [54]

$$\mathbf{b} = [R]\left([I] - [H][R]\right)^{-1}\mathbf{H}_S b_s, \tag{9}$$

with $[I]$ being the identity matrix. Hence, through Eq. (9), the term $d\mathbf{b}/d\mathbf{\Phi}$ in Eq. (6) can now be analytically calculated for an infinite number of interactions between unit cells [49].

It is evident that if we know all the Green's function values for Eqs. (7)–(9), we can find the desired gradient from Eq. (6) and then begin the optimization solver for the specific problem. These Green's function matrix or vector elements can be either obtained via either numerical simulations or measurements in a preoptimization step or analytically calculated for certain environments.

III. FOCUSING APPLICATIONS

We now apply the proposed topology-optimization technique to various 2D focusing problems involving a reconfigurable metasurface in a complex medium. First, we apply the proposed technique for a tunable metasurface in free space, where the Green's functions required are replaced by the analytical free-space 2D ones. Next, we optimize the focusing problem for a reconfigurable metasurface placed inside a complex environment mimicking an office room, which takes the form of a leaky cavity. In this case, the Green's functions are not known; therefore, they are extracted via numerical simulations before the optimization technique is applied. This acquisition step is time-consuming, but once all the Green's functions are known, the optimization is quick. Finally, we address the problem of a leaky-cavity antenna, where the metasurface and the source are placed in a partially open reverberating cavity. For this specific geometry, the 2D Green's functions can be analytically calculated.

Whenever the Green's functions are needed to be extracted or a visualization of the results is required, we use COMSOL MULTIPHYSICS as a simulation tool. In particular, each example is reconstructed in COMSOL MULTIPHYSICS in the manner in Fig. 1, and the equivalent sources replacing the metasurface unit cells are set up as a function of the retrieved phases, where $b_i(\phi_i) = R_i(\phi_i)\mathbf{E}_i^{\text{loc}}$, as explained in Sec. II A.

In all problems, we perform the required optimization exploring two cases: taking into account infinite interactions or no interactions between the elements of the metasurface. The latter is the more common in metasurface models [11,25] due to the simplicity it offers for modeling. Nevertheless, it is expected to produce worse maxima for the optimization problem in comparison with the full interaction model, especially as the environment complexity increases. Infinite interactions are considered if one uses Eq. (9), while no interaction is included if Eq. (8) is used with $n = 0$. Finally, the resulting phase sets, $\mathbf{\Phi}_\infty$ and $\mathbf{\Phi}_0$, for, respectively, the infinite-interaction and no-interaction cases are inserted into the full model of Eq. (7) and are compared for their intensity outputs.

Finally, we choose to work in the microwave spectrum, in which many applications on wireless communications involving reconfigurable metasurfaces are used, both outdoors and indoors [4,5,10,11]. Thus, the operational frequency f is set to 2.4 GHz, while the distance d between the elements of the metasurface is chosen as $\lambda/2$ to have Shannon sampling of the metasurface [23,24]. Nevertheless, the procedure presented is general, and it can be used for smaller element distances, as well as other frequencies and applications, e.g., imaging with light using SLMs [18].

A. Free space

We first apply the proposed optimization technique to the simplest case for the setup illustrated in Fig. 1, where the "complex medium" is replaced by free space. This specific case enables a fast and easy analytical approach. First, the Green's functions H_{Fi} and H_{Si} required for the calculations with Eq. (7) have an analytical expression [45,56] (see Appendix A). Second, in the absence of a complex, reflective or absorbing environment, only the direct interaction between the metasurface elements exists, and thus the H_{ij} are also the analytical textbook's formulas, which depend only on the distance between i and j. All field calculations via Green's functions are performed in the far field, or at least for distances greater than $\lambda/2$, i.e., the unit-cell dimension.

In this example, we use a metasurface of $N = 101$ reconfigurable elements or design variables; the center of the metasurface is placed at the origin of the axes, $O(0, 0)$. Moreover, we place a point source with $I_S = 1$ A at the point $S(20\lambda, 5\lambda)$. The optimization goal is arbitrarily set as the maximization of the intensity at the point $F(-15\lambda, 60\lambda)$, as formulated in Eq. (2). The values of the binarization parameters are set as $\alpha = 30$, $\beta = 2$, and $\beta_{\text{inc}} = 2$, as detailed in Sec. II B.

The proposed topology-optimization method is applied for this free-space example, for cases of infinite interactions and no interactions between the metasurface elements. After the desired phase set is analytically computed, the phase set from the infinite-interaction analysis, $\mathbf{\Phi}_\infty$, is inserted into the COMSOL MULTIPHYSICS simulation; the resulting electric field intensities are depicted in Fig. 2(a). A focus is achieved at the expected point F.

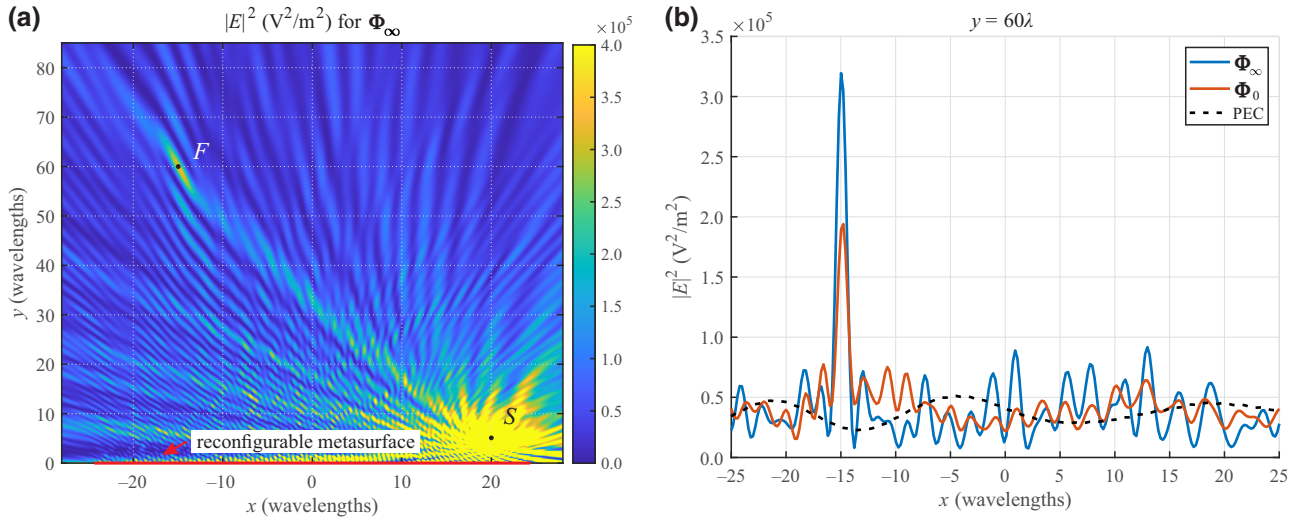

FIG. 2. Free-space problem. (a) Mapping of the intensities via COMSOL MULTIPHYSICS simulation, with the phase set $\mathbf{\Phi}_\infty$ as input. (b) Electric field intensities for $y = 60\lambda$ and the various phase sets obtained by the proposed topology-optimization process.

We now compare the efficiency between the use of infinite interactions and the use of zero interactions, using the 2D Green's functions for free space to analytically calculate $|E|^2$ for $y = 60\lambda$ via Eq. (7). At these points the electric field is calculated by taking into account all the metasurface-element interactions, for each phase-set solution. Comparative results obtained with $\mathbf{\Phi}_\infty$ and $\mathbf{\Phi}_0$ optimization solutions, as well as results obtained with $\phi_i = \pi$ for each element, thus emulating a metallic reflector, are displayed in Fig. 2(b). The final focus at $x = -15\lambda$ is clearly observed for both retrieved phase sets; however, a relative improvement of 70% is calculated between zero interactions and infinite interactions. Moreover, the relative improvement between the perfect-electrical-conductor (PEC) reflector and the $\mathbf{\Phi}_\infty$ solution is approximately 1200%. The resulting phase sets from the optimization algorithm along with the comparison between the analytical intensity calculations and the simulations are provided in Ref. [49].

The improvement in the final intensity at the focusing point obtained with infinite interactions in comparison with zero interactions is relatively small for a free-space problem but is still non-negligible. Therefore, the approximation, commonly used in reconfigurable-metasurfaces applications, of not considering it, is relatively efficient for free-space setups. Nevertheless, as we see in the following examples, highly reflective and complex environments deem the inclusion of the element interactions via the matrix $[H]$ in Eq. (8) necessary for a large focusing effect in the optimization process.

B. Complex leaky cavity

Next, the optimization algorithm is applied on a truly complex and random environment: a leaky room. This complex medium, depicted in Fig. 3(a), is modeled as a 2D orthogonal leaky cavity containing PEC obstacles of different shapes. Obviously, in this case, the 2D Green's functions cannot be obtained analytically. Thus, the 2D Green's functions are extracted via simulations with COMSOL MULTIPHYSICS. Specifically, the H_{ij} are obtained by our placing a point source with amplitude $I_i = 1$ A at the position of each element i and measuring the electric field at the positions of the other j elements, thus running N independent simulations. From the same simulations, the values of $\mathbf{H}_F$ and $\mathbf{H}_S$ are also obtained. For H_{FS}, an $(N+1)$th simulation is required. The values of H_{ii} are not extracted herein, and they are approximated as zeros. This procedure for extracting 2D Green's functions via simulations requires much computational time, especially for a dense mesh. However, the values are characteristic of the problem's geometry and can be stored and used in future optimization runs. Specifically, if the source point and the metasurface position are fixed and the focusing point is moving, as in the case of a stationary WiFi router in a room communicating with a moving device, the $[H]$ and $\mathbf{H}_S$ values are already pre-extracted and stored and only a single simulation is required for the retrieval of $\mathbf{H}_F$ and H_{FS} as long as the rest of the environment does not change. Moreover, the same procedure for the 2D Green's functions retrieval can be performed via measurements much faster, provided that the elements of the metasurfaces and the receiver at the focusing point have receiver/transmitter capabilities.

Again, as in the previous example, we use a metasurface of $N = 101$ reconfigurable elements/design variables placed at the origin of the axes. The source with $I_S = 1$ A is placed at $S(20\lambda, 5\lambda)$ and the focusing point is at $F(-15\lambda, 60\lambda)$, just like in the previous free-space problem. The values of the binarization parameters are

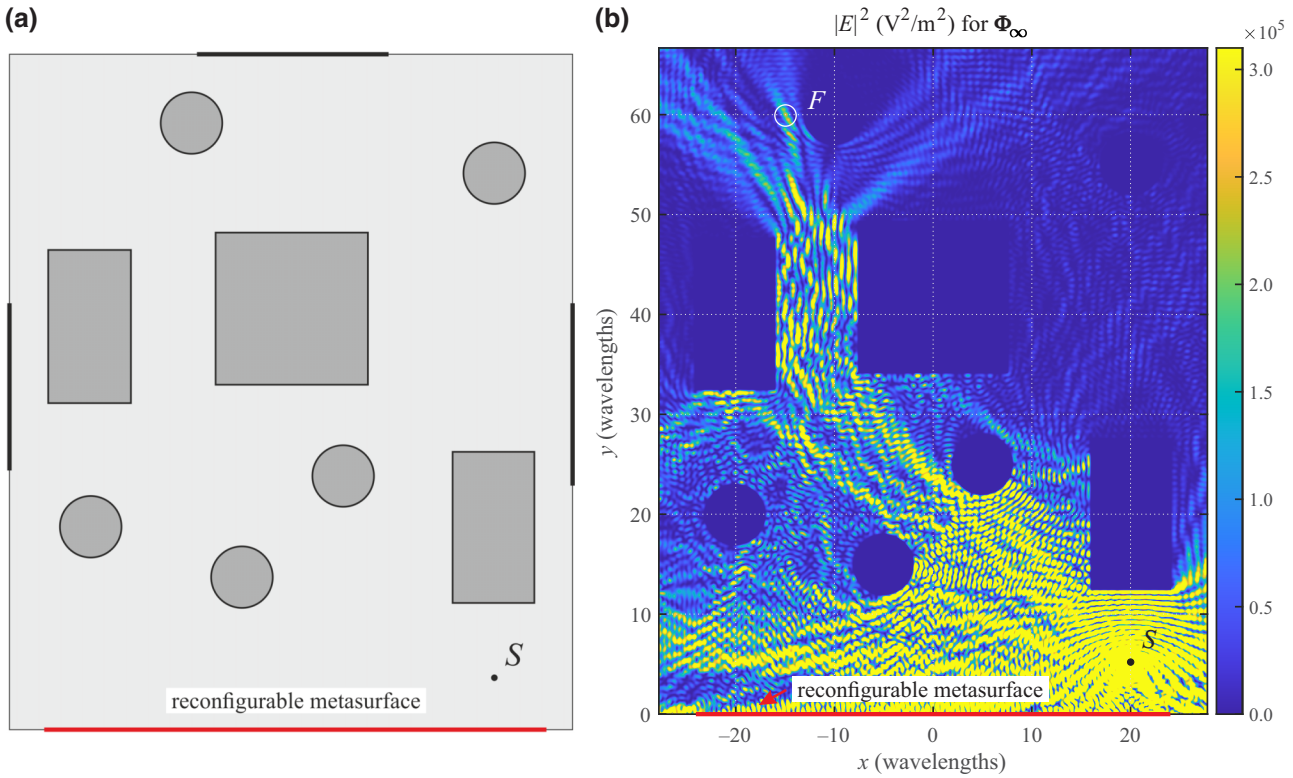

FIG. 3. Complex leaky-cavity problem. (a) The leaky cavity/room: The surfaces of the circular and square obstacles are made of a PEC. The boundaries of the cavity are constructed via the "transition boundary condition" of COMSOL MULTIPHYSICS, with the bold lines representing "windows" with material parameters $\varepsilon_r = 1.5$, $\mu_r = 1$, and $\sigma = 0$ and with thickness equal to λ, and with the normal lines representing "walls" with material parameters $\varepsilon_r = 5$, $\mu_r = 1$, and $\sigma = 0$ and with thickness equal to 2λ. The dimensions of the cavity are set as $W \times H = 1.1Nd \times 1.32Nd$. (b) Mapping of the intensities via COMSOL MULTIPHYSICS simulation, with the phase set $\mathbf{\Phi}_\infty$ as input.

set as $\alpha = 40$, $\beta = 1.2$, and $\beta_{\text{inc}} = 1.2$, as explained in Sec. II B.

Once all 2D Green's functions are extracted via simulations, the proposed topology optimization is then used for both $n = 0$ and $n \to \infty$ element interactions in Eq. (8). The resulting intensity inside the cavity for the optimal phase solutions for infinite interactions is depicted in Fig. 3(b). F appears to be on a region of increased intensity compared with neighboring points. The intensity around F is also depicted in Fig. 4(a), where the resulting focus is more clearly shown. In parallel, the absence of focusing around F when a random set of phases is used is illustrated in Fig. 4(b). The relative change in intensity between the random phase set and the infinite-interaction phase set is roughly 4000%. Finally, the relative improvement for the intensity between the zero-interaction solution and the infinite-interaction solution is a factor of 3.5. The resulting phase-set solution from the topology-optimization process and the intensities along the lines $x = -15\lambda$ and $y = 60\lambda$ are provided in Ref. [49].

In this complex environment, once the set of Green's functions is fully known, the optimization procedure is very quick and finds a solution that effectively exhibits a focus near the target position F. The overall improvement is far better than in free space, thus making the use of RISs all the more interesting when used in a complex and reverberating environment where each pixel provides an extra degree of freedom [18,57]. Note that the inclusion of infinite interactions between the elements of the reconfigurable metasurface is mandatory as it has provided a solution that results in a considerably better focus in comparison with not including the interactions. However, in this example, the improvement comes with a considerable cost of the computationally demanding pre-extraction of the matrix $[H]$.

To tackle this issue, we propose finding a geometry of a complex medium where H_{ij}, $\mathbf{H}_F$, $\mathbf{H}_S$, and H_{FS} can be precalculated analytically, thus providing speed in the topology-optimization process. In the next example, we examine one such case.

C. Cavity antenna

For the last example, we apply the proposed topology-optimization algorithm to another complex and highly reflective environment, but this time where the necessary

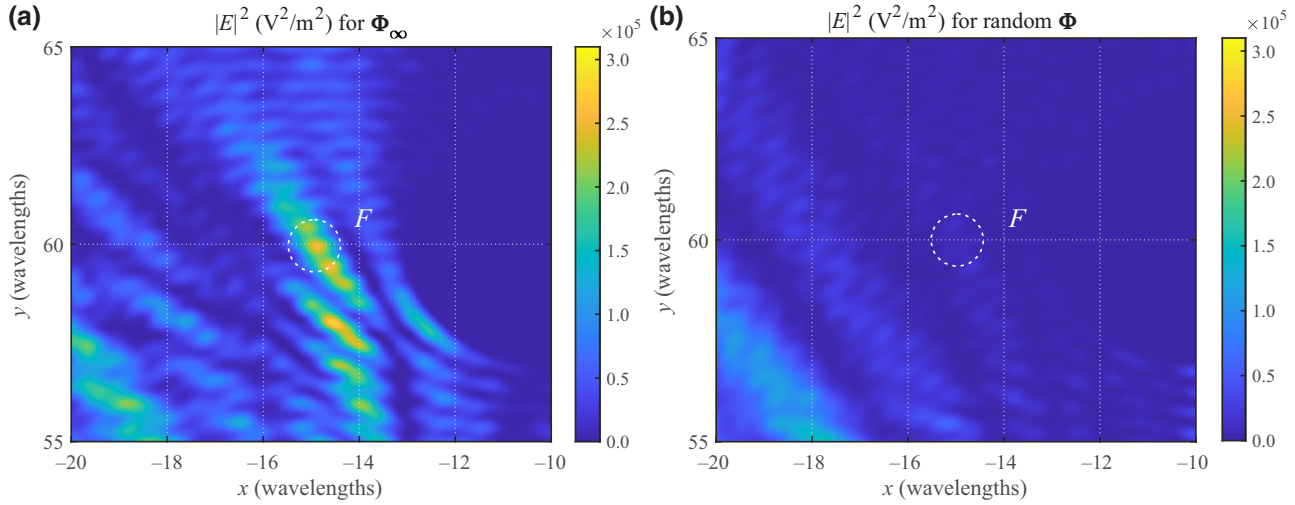

FIG. 4. Complex leaky-cavity problem. Mapping detail of the intensities via COMSOL MULTIPHYSICS simulation around the focusing point (a) for phase set $\mathbf{\Phi}_\infty$ and (b) for a random phase set.

2D Green's functions are analytically calculated. Such a geometry consists of a 2D cavity antenna as depicted in Fig. 5(a). The RIS is placed at the bottom of a reverberating cavity, with the right and left walls of the cavity being made of perfectly conducting material. The fourth wall (top) is made of a partially reflective surface, which is composed of a subwavelength metallic grating (alternation of metal and free space); thus, the cavity leaks to the surrounding environment. The source feed is placed inside the cavity itself. The focusing point is placed outside the 2D leaky cavity. This type of device constitutes a cavity antenna, used as an example in this subsection, and has attracted considerable attention both in academia and industry for applications involving, for example, satellite communications and radar [58,59].

The key point of this example is the analytical calculation of the 2D Green's functions, which practically corresponds to the calculation of fields inside and outside the cavity. First, the reflection and transmission coefficients from an infinite version of the partially reflective aperture are calculated for plane-wave incidence and angle range $(-\pi, \pi)$. For the specific case of a 2D aperture array, the

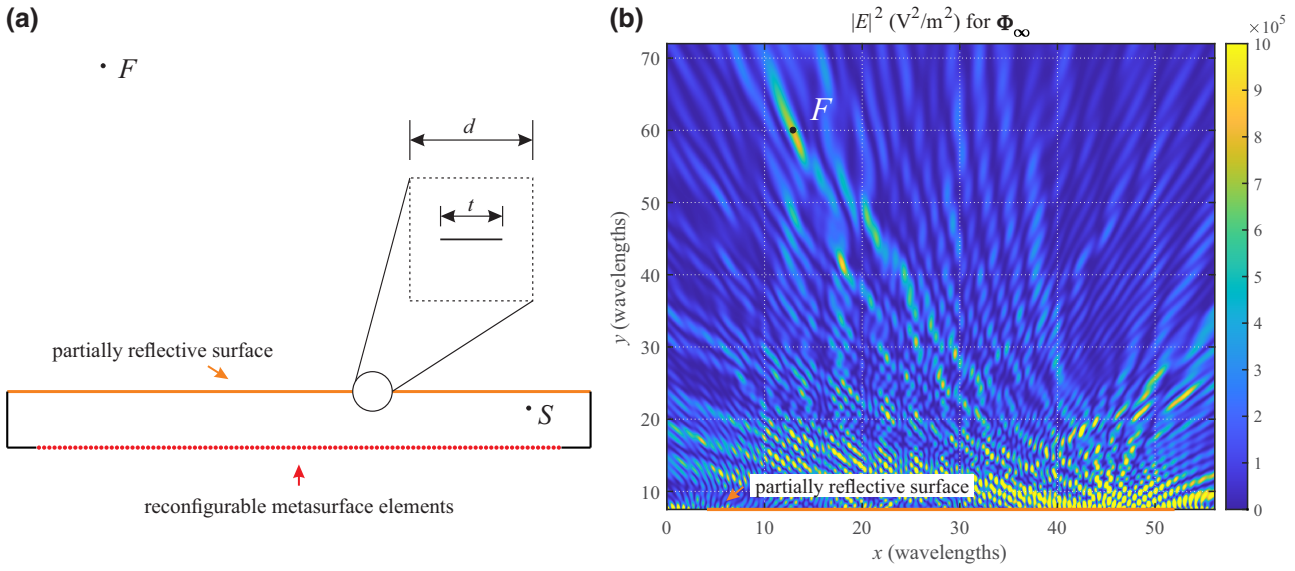

FIG. 5. Cavity-antenna problem. (a) The cavity-antenna design. The height h of the cavity is set to 7.5λ, while its length L is $1.1(N+1)d$, with d being the unit-cell dimension. The inset shows an illustration of the unit cell of the partially reflective surface. The unit-cell dimension d is set to $\lambda/2$, while a PEC strip placed is the middle of the unit cell with dimension $t = 0.2d$. (b) Mapping of the intensities via COMSOL MULTIPHYSICS simulation, with the phase set $\mathbf{\Phi}_\infty$ as input.

reflection and transmission coefficients can be analytically calculated [45], or they can be extracted via simulations, as we do specifically in this work. Afterwards, the calculation of the fields inside the cavity leads to the calculation of H_{ij} and H_{Si}. In particular, for this purpose, we use the *method of images* to remove the walls of the cavities and calculate the fields inside via summations of 2D free-space Green's functions, taking into account as many images of the sources as required to achieve adequate convergence. Finally, to evaluate the field outside the cavity, *Kirchhoff's integral theorem* is used. From the fields on the partially reflective surface, the fields outside the cavity are obtained, and thus the required values of H_{Fi} and H_{FS} are obtained. The formulas for the analytical calculation of the 2D Green's functions for this cavity-antenna example are provided in Appendix B, while a more-detailed analysis of their derivation is given in Ref. [49]. As for the example in Sec. III A, all field calculations are performed in the far field.

We again use $N = 101$ elements with 0 or π phase states, and the bottom-left corner of the cavity is placed at $O(0, 0)$, as depicted in Fig. 5(a). After placing a source at the point $S(48.05\lambda, 5\lambda)$ and setting the optimization goal to be focusing at the point $F(13.05\lambda, 60\lambda)$, we apply the proposed topology-optimization technique to the problem for the cases of infinite and zero element interactions. The values of the binarization parameters are set as $\alpha = 40$, $\beta = 1$, and $\beta_{\text{inc}} = 1.2$, as explained in Sec. II B. The optimization is fully run in MATLAB with these analytical formulae, and then the optimal phase solutions are reinjected into COMSOL MULTIPHYSICS to visualize the field distribution outside the cavity.

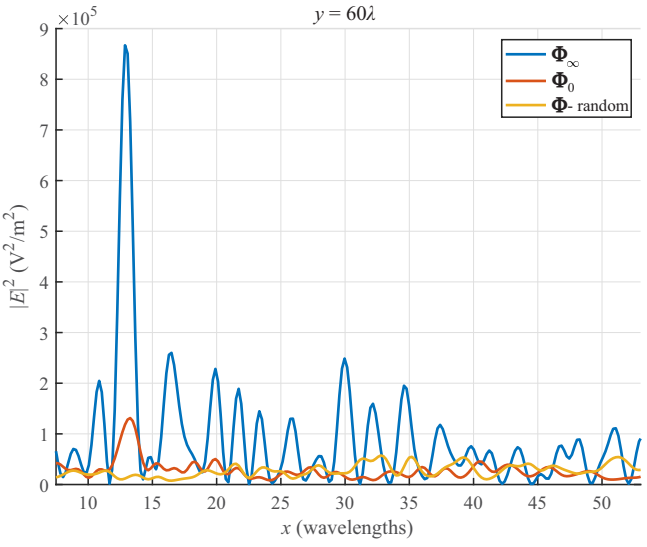

FIG. 6. Cavity-antenna problem. The electric field intensities for $y = 60\lambda$ and the various phase sets obtained with the proposed topology-optimization process.

The mapping of the intensities above the partially reflective surface for the resulting $\mathbf{\Phi}_\infty$ set is provided in Fig. 5(b). A focus is successfully created at the expected point F, confirming that both the analytical formulae and the topological optimization have worked. Comparative results for $|E|^2$ at $y = 60\lambda$ obtained with the infinite-interaction and zero-interaction optimization solutions, as well as results obtained with a random pick of 0 or π phase values, are displayed in Fig. 6. The relative intensity change between the random phase set and the $\mathbf{\Phi}_\infty$ set at the focus at $x = 13.05\lambda$ is calculated to be roughly 70 000%, while the relative intensity change between the $\mathbf{\Phi}_0$ set and the $\mathbf{\Phi}_\infty$ set shows an improvement of more than 6 times.

D. Discussion

From all the previous examples, we can first conclude that the topology-optimization scheme manages to find optimal binary phase solutions that effectively create a focus. The focusing results are expected to improve with a larger number of reconfigurable elements or, in other words, a larger number of design variables/degrees of freedom. Also, as the complexity of the medium increases, the improvement in the resulting focusing becomes all the more remarkable. This is a direct consequence of the complexity of the medium, which we leverage to our advantage by being able to control the spatial degrees of freedom [10,18,57]. The more complex the environment, the more useful the RIS. Or said differently, the more "multipath" the different Green's functions are, the more impact each individual pixel has.

The second comment is a corollary of the previous one. As the Green's function becomes more and more complex together with the propagating medium, there are more chances that waves are reflected back to the other pixels of the metasurface. Therefore, a big difference is made in the algorithm on whether multiple interactions between the pixels are considered. Indeed, for the case of a metasurface in free space, the topology-optimization results provide a barely better focus for infinite interactions in comparison with zero interactions. Therefore, the latter option is potentially viable for the common free-space, telecommunication examples [4]. However, it is later shown that the use of $n \to \infty$ in Eq. (8) instead of $n = 0$ provides visibly better results. Specifically, as the environment becomes increasingly more reflective and involves more modes [11], the use of infinite interactions is essential to obtain a focus via the proposed topology-optimization scheme. Interestingly, in terms of computational demands, it is more efficient since only a single matrix inversion is required, as shown in Eq. (9).

Third, an important feature that greatly enhances the performance of the presented topology-optimization technique is the prospect of the analytical calculation of the

required 2D Green's function values in Eq. (7) for certain geometries. In principal, the Green's functions values can always be extracted via simulations in a preoptimization step, as demonstrated in the leaky-room example in Sec. III B. In practice, though, this requires a lot of computational time and resources, and even if the values of $[H]$ and $\mathbf{H}_S$ characterize the geometry of a time-invariant complex medium, and can be stored and reused for multiple optimization runs, one must still extract each time the values of $\mathbf{H}_F$ and H_{FS} for a changing position of the desired focusing point F. However, this problem is alleviated if the geometry of the complex medium permits an analytical calculation of the Green's function, as performed in the example in Sec. III C. This not only obviously enables a much-faster overall optimization process, but also enables a real-time experimental use of topology optimization, which is particularly useful for telecommunication applications, where the focusing point/receiver constantly changes position [11,59]. The confirmation of the analytical solution with simulation was performed here, but undoubtedly the next step will be to test this scenario experimentally.

Regarding the benefits of the proposed method in comparison with alternatives, obviously use of the adjoint method for gradient retrieval instead of an explicit numerical calculation results in a huge improvement in terms of speed and computational burden. Furthermore, the use of the Green's function formulation of the problem herein, especially if the Green's functions can be acquired analytically, greatly helps the adjoint method itself, because this time the direct and adjoint solutions are not obtained by means of two finite-element-method or finite-difference-time-domain simulations for each iteration, as commonly done in related applications [30,34]. Therefore, the optimization process is fast. Even if the Green's functions cannot be analytically retrieved (Sec. III B), the Green's function formulation for the optimization problem is still beneficial, as the required Green's functions are extracted via simulations at the beginning, and then all iteration steps are performed rapidly. Because the Green's function values are geometry dependent, they can be stored and used for another optimization cycle, on the same setup. In comparison with the non-gradient-based optimization methods, as mentioned in Sec. I, the gradient-based optimization methods generally perform better in terms of convergence times when many degrees of freedom are involved [30]. In particular, in the example in Ref. [10], the optimization method used was a nongradient one and was based on a simple concept: Before the initial iteration all elements on the metasuface are set to the 0 phase value. Then each element is iteratively switched to the π phase and the intensity is measured at the desired focusing point. If the resulting intensity is higher, the element is kept with π, otherwise it is changed back to 0. This procedure is repeated until convergence is achieved, but it is highly inefficient and could take for hours for 102 elements or variables, while the method proposed in this work can result in convergence in approximately 1 minute for 101 elements or variables. The applicability of the proposed topology-optimization method is not confined to the example in Ref. [30], which is similar to the example in Sec. III B, and the method can also be used for free-space problems (Sec. III A), cavity antennas (Sec. III C), and possibly other cases.

Considering future endeavors, although the analysis presented herein is formulated and performed for 2D problems, it is general in nature and can be extended, with some care, to 3D complex media. Apart from the different types of Green's function that must be used (see Appendix A), one has to also take into account for the 3D cases the different polarizations, the different multipole types (electric and magnetic), and the choice of the multipolar order. These considerations will eventually produce more-complicated matrices and vectors in the respective equation (7) for 3D environments, but the formalism should remain valid. Moreover, the SMMs used herein can switch between only two states, but other types of element, i.e., the SLMs used in optics and imaging applications, could potentially have multiple states. In that case, our proposed method requires an extension. Specifically, the current scheme is confined to two states because of the basic idea stemming from topology optimization in photonics, which is the design of structures that either are filled or not filled by material, i.e., a final "black-and-white" structure. To include more than two states, one would have come up with a new, continuous, and derivable filter function in place of the smoothed Heaviside function used. Finally, in this work the elements were considered as point scatterers, which radiate isotropically in 2D space. This was done for simplicity, yet without loss of generality. As a future step forward, one could add near fields in the model, as well as higher-order multipoles [24], taking into account that the calculations involving the required Green's function values in Eqs. (7) and (8) will be more complicated.

IV. CONCLUSION

In this paper, we have presented a topology-optimization technique to perform electromagnetic focusing when binary reconfigurable metasurfaces are used in complex media. First, the optimization problem was formulated in two dimensions, with the elements of the metasurface approximated as point sources and with the use of Green's functions. Moreover, the adjoint method was used for the fast retrieval of the necessary derivative. Subsequently, the method developed was applied to various focusing examples in complex environments for 2D Green's function values analytically calculated or retrieved via simulations. The obtained phase values of the reconfigurable elements provided excellent focusing at the intended points, while

it was also demonstrated that the consideration of infinite interactions between metasurface elements in the topology-optimization scheme provides significantly large intensities at the focus.

For future work, we aim to expand the proposed topology-optimization technique to 3D problems involving complex media, as well as to experimentally use the presented technique for real-time free-space or cavity problems. Additionally, we plan to add more scatterer models to represent in our method more-realistic and more-complicated metasurface elements.

ACKNOWLEDGMENTS

T.K. thanks Yannick Augenstein for long and fruitful discussions on the theory and algorithms of topology optimization. We thank Steven Johnson for introducing us to the vast world of topology optimization. This work has received support under the program "Investissements d'Avenir" launched by the French Government, from the Simons Collaboration on Symmetry-Driven Extreme Wave Phenomena, and from the "Agence de l'Innovation de Defense" under the RAPID m3SFA project.

APPENDIX A: TWO-DIMENSIONAL GREEN'S FUNCTION FOR FREE SPACE

Let us consider a 2D space, described by the cylindrical coordinate system (ρ, θ) and with the vector to an observation point $\boldsymbol{\rho} = \rho\hat{\boldsymbol{\rho}} = x\hat{\mathbf{x}} + y\hat{\mathbf{y}} = \rho\left(\cos\theta\hat{\mathbf{x}} + \sin\theta\hat{\mathbf{y}}\right)$. A unitary point source is placed at $\boldsymbol{\rho}'$ with an imposed current along the $\hat{\mathbf{z}}$ direction. Additionally, the medium is inhomogeneous, but it does not affect the polarization of the propagating waves. Hence, the problem is described by the Helmholtz equation:

$$\left(\nabla^2 + \frac{\omega^2}{c^2(\boldsymbol{\rho})}\right) H(\boldsymbol{\rho}, \boldsymbol{\rho}')\hat{\mathbf{z}} = -\delta(\boldsymbol{\rho} - \boldsymbol{\rho}')\hat{\mathbf{z}}. \tag{A1}$$

The solution to this problem $H(\boldsymbol{\rho}, \boldsymbol{\rho}')$ is called the Green's function. For the case of unbounded, homogeneous *free space*, it is the perpendicular 2D Green's function [56]:

$$H(\boldsymbol{\rho}, \boldsymbol{\rho}') = G_{2D}(\|\boldsymbol{\rho} - \boldsymbol{\rho}'\|) = -\frac{\mathrm{i}}{4}H_0^{(2)}(kR), \tag{A2}$$

where $H_0^{(2)}(.)$ denotes the zeroth-order Hankel function of the second kind, $k = \omega/c$ is the free-space wave number, and $R = \|\boldsymbol{\rho} - \boldsymbol{\rho}'\|$.

APPENDIX B: CALCULATION OF $[H]$, $\mathbf{H}_F$, $\mathbf{H}_S$, AND H_{FS} FOR THE CAVITY-ANTENNA PROBLEM

The problem under study is the leaky cavity antenna depicted in Fig. 5(a). The application of the proposed topology-optimization technique requires the calculation of the Green's function values in Eqs. (7) and (9). The reflection and transmission coefficients at the partially reflective surface, or simply r and t, are a function of the angle θ of the incident wave and can be either calculated or extracted via simulations.

To emulate the presence of the walls, the method of images is applied [45,56]. The metasurface elements are placed exactly at the bottom of the cavity and therefore there is no reflection on the bottom wall. Then, the H_{ij} and H_{Si} can be calculated analytically. The H_{ij} are calculated as

$$H_{ij}^d = \sum_{-m}^{m}\left\{G_{2D}(d_{ij,m}^+) - G_{2D}(d_{ij,m}^-)\right\}, \quad i \neq j, \tag{B1a}$$

$$H_{ij}^r = \sum_{-m}^{m}\left\{r(\theta_{ij,m}^+)G_{2D}(q_{ij,m}^+) - r(\theta_{ij,m}^+)G_{2D}(q_{ij,m}^-)\right\}, \quad i \neq j, \tag{B1b}$$

$$H_{ij} = H_{ij}^d + H_{ij}^r, \tag{B1c}$$

where $d_{ij,m}^{\pm} = |x_j - (\pm x_i + 2mL)|$, $\theta_{ij,m}^{\pm} = \tan^{-1}(d_{ij,m}^{\pm}/2h)$, and $q_{ij,m}^{\pm} = \sqrt{4h^2 + (d_{ij,m}^{\pm})^2}$, with $m \in \mathbb{Z}$, according to Fig. 5(a). x_i and x_j correspond to the x coordinates of the unit-cell centers. Moreover, $|m|$ indicates the number of images considered in the analysis. Because G_{2D} stands for a cylindrical wave, the further away the source, the lower the magnitude of the Green's function, therefore $|m| = 20$–30 provides very good accuracy.

The elements of the main diagonal of $[H]$ are themselves calculated as

$$H_{ii} = r(0)G_{2D}(2h) + \sum_{-m}^{m}\left\{G_{2D}(d_{ii,m}^+) - G_{2D}(d_{ii,m}^-)\right\}. \tag{B2}$$

The H_{Si} are similarly calculated as

$$H_{Si}^d = \sum_{-m}^{m}\left\{G_{2D}(q_{1,i,m}^+) - G_{2D}(q_{1,i,m}^-)\right\}, \tag{B3a}$$

$$H_{Si}^r = \sum_{-m}^{m}\left\{r(\theta_{Si,m}^+)G_{2D}(q_{2,i,m}^+) - r(\theta_{Si,m}^+)G_{2D}(kq_{2,i,m}^-)\right\}, \tag{B3b}$$

$$H_{Si} = H_{Si}^d + H_{Si}^r, \tag{B3c}$$

where $d_{Si,m}^{\pm} = |2mL \pm x_S - x_i|$, $\theta_{Si,m}^{\pm} = \tan^{-1}(d_{Si,m}^{\pm}/(2h - y_S))$, $q_{1,i,m}^{\pm} = \sqrt{y_S^2 + (d_{Si,m}^{\pm})^2}$, and $q_{2,i,m}^{\pm} = \sqrt{(2h^2 - y_S)^2 + (d_{Si,m}^{\pm})^2}$, with $m \in \mathbb{Z}$.

Afterwards, the calculation of the remaining values of H_{Fi} and H_{FS} requires the accurate calculation of the fields

outside the cavity. This is possible by use of the *Kirchhoff integral* [45,60], where all infinitesimally small sections of the partially reflective surface of the problem in Sec. III C are considered to be point sources. Therefore, the integral is transformed for the current problem in Fig. 5(a) as

$$E(\boldsymbol{\rho}_F) = \int_0^L E(\boldsymbol{\rho}')\left(\hat{\mathbf{y}}\cdot\nabla' G_{2\mathrm{D}}\left(\|\boldsymbol{\rho}_F-\boldsymbol{\rho}'\|\right)\right) + G_{2\mathrm{D}}\left(\|\boldsymbol{\rho}_F-\boldsymbol{\rho}'\|\right)\left(\hat{\mathbf{y}}\cdot\nabla' E(\boldsymbol{\rho}')\right)\mathrm{d}x, \quad \text{(B4)}$$

where the vector $\boldsymbol{\rho}'$ represents the position of each piece of the integral, while $\boldsymbol{\rho}_F$ represents the position of the point where the field is to be calculated, herein the focusing point. Hence, $\|\boldsymbol{\rho}_F-\boldsymbol{\rho}'\| = R_F = \sqrt{(x_F-x')^2+(y_F-h)^2}$. The right-hand side of Eq. (B4) is reformulated as

$$\hat{\mathbf{y}}\cdot\nabla' G_{2\mathrm{D}}(R_F) = \frac{|y_F-h|}{\sqrt{(x_F-x')^2-(y_F-h)^2}}\left[\frac{\mathrm{i}k}{4}H_1^{(2)}(kR_F)\right]. \quad \text{(B5)}$$

The problem of calculating H_{Fi} and H_{FS} essentially becomes a problem of calculating the electric fields and their derivatives on each point of the partially reflective surface. Specifically, the electric field at F is calculated with Eq. (B4) after placement of a current point source at the positions of metasurface elements or at S and with use of the method of images. Therefore, for each metasurface element i, it is derived that

$$E_{ix'} = \sum_{-m}^{m}\left\{t(\theta^+_{ix',m})G_{2\mathrm{D}}(u^+_{i,m}) - t(\theta^-_{ix',m})G_{2\mathrm{D}}(u^-_{i,m})\right\} \times(-\mathrm{i}\omega\mu I_i), \quad \text{(B6a)}$$

$$\hat{\mathbf{y}}\cdot\nabla' E_{ix'} = \frac{-\mathrm{i}k}{4}\sum_{-m}^{m}\left\{\frac{h}{u^+_{i,m}}t(\theta^+_{ix',m})H_1^{(2)}(ku^+_{i,m}) - \frac{h}{u^-_{i,m}}t(\theta^-_{ix',m})H_1^{(2)}(ku^-_{i,m})\right\}(-\mathrm{i}\omega\mu I_i), \quad \text{(B6b)}$$

where $u^\pm_{i,m} = \sqrt{h^2+(x'+2mL\pm x_i)^2}$ and $\theta^\pm_{ix',m} = \tan^{-1}(u^\pm_{i,m}/h)$, with $m\in\mathbb{Z}$. Similarly, for the source point S, it holds that

$$E_{Sx'} = \sum_{-m}^{m}\left\{t(\theta^+_{Sx',m})G_{2\mathrm{D}}(u^+_{S,m}) - t(\theta^-_{Sx',m})G_{2\mathrm{D}}(u^-_{S,m})\right\}(-\mathrm{i}\omega\mu I_i), \quad \text{(B7a)}$$

$$\hat{\mathbf{y}}\cdot\nabla' E_{Sx'} = \frac{-\mathrm{i}k}{4}\sum_{-m}^{m}\left\{\frac{h}{u^+_{S,m}}t(\theta^+_{Sx',m})H_1^{(2)}(ku^+_{\mathrm{S},m}) - \frac{h}{u^-_{S,m}}t(\theta^-_{Sx',m})H_1^{(2)}(ku^-_{\mathrm{S},m})\right\}(-\mathrm{i}\omega\mu I_i), \quad \text{(B7b)}$$

where $u^\pm_{S,m} = \sqrt{(y_S-h)^2+(x'+2mL\pm x_S)^2}$ and $\theta^\pm_{Sx',m} = \tan^{-1}(u^\pm_{S,m}/(y_S-h))$, with $m\in\mathbb{Z}$. Insertion of Eqs. (B5), (B6a), and (B6b) into Eq. (B4) produces E_{Fi}, which in turn leads to the calculation of the vector element $H_{Fi} = E_{Fi}/(-\mathrm{i}\omega\mu I_i)$. Finally, insertion of Eqs. (B5), (B7a), and (B7b) into Eq. (B4) gives E_{FS}, which is required for Eq. (7), $H_{FS} = E_{FS}/(-\mathrm{i}\omega\mu I_i)$.

[1] I. M. Vellekoop and A. Mosk, Focusing coherent light through opaque strongly scattering media, Opt. Lett. **32**, 2309 (2007).

[2] V. Cecconi, V. Kumar, A. Pasquazi, J. S. T. Gongora, and M. Peccianti, Nonlinear field-control of terahertz waves in random media for spatiotemporal focusing, Open Res. Europe **2** (2023).

[3] O. Katz, E. Small, Y. Bromberg, and Y. Silberberg, Focusing and compression of ultrashort pulses through scattering media, Nat. Photonics **5**, 372 (2011).

[4] M. Di Renzo, K. Ntontin, J. Song, F. H. Danufane, X. Qian, F. Lazarakis, J. De Rosny, D.-T. Phan-Huy, O. Simeone, R. Zhang, *et al.*, Reconfigurable intelligent surfaces vs. relaying: Differences, similarities, and performance comparison, IEEE Open J. Commun. Soc. **1**, 798 (2020).

[5] O. Tsilipakos, A. C. Tasolamprou, A. Pitilakis, F. Liu, X. Wang, M. S. Mirmoosa, D. C. Tzarouchis, S. Abadal, H. Taghvaee, C. Liaskos, *et al.*, Toward intelligent metasurfaces: The progress from globally tunable metasurfaces to software-defined metasurfaces with an embedded network of controllers, Adv. Opt. Mater. **8**, 2000783 (2020).

[6] G. C. Alexandropoulos, N. Shlezinger, and P. Del Hougne, Reconfigurable intelligent surfaces for rich scattering wireless communications: Recent experiments, challenges, and opportunities, IEEE Commun. Mag. **59**, 28 (2021).

[7] C. Huang, A. Zappone, G. C. Alexandropoulos, M. Debbah, and C. Yuen, Reconfigurable intelligent surfaces for energy efficiency in wireless communication, IEEE Trans. Wirel. Commun. **18**, 4157 (2019).

[8] E. Basar, M. Di Renzo, J. De Rosny, M. Debbah, M.-S. Alouini, and R. Zhang, Wireless communications through reconfigurable intelligent surfaces, IEEE Access **7**, 116753 (2019).

[9] M. A. ElMossallamy, H. Zhang, L. Song, K. G. Seddik, Z. Han, and G. Y. Li, Reconfigurable intelligent surfaces for wireless communications: Principles, challenges, and opportunities, IEEE Trans. Cogn. Commun. Netw. **6**, 990 (2020).

[10] N. Kaina, M. Dupré, G. Lerosey, and M. Fink, Shaping complex microwave fields in reverberating media with binary tunable metasurfaces, Sci. Rep. **4**, 6693 (2014).

[11] M. Dupré, P. Del Hougne, M. Fink, F. Lemoult, and G. Lerosey, Wave-field shaping in cavities: Waves trapped in a box with controllable boundaries, Phys. Rev. Lett. **115**, 017701 (2015).

[12] P. Del Hougne, F. Lemoult, M. Fink, and G. Lerosey, Spatiotemporal wave front shaping in a microwave cavity, Phys. Rev. Lett. **117**, 134302 (2016).

[13] J. B. Gros, G. Lerosey, F. Lemoult, M. Lodro, S. Greedy, and G. Gradoni, Multi-path fading and interference mitigation with reconfigurable intelligent surfaces, arXiv:2206.08290.

[14] M. F. Imani, J. N. Gollub, O. Yurduseven, A. V. Diebold, M. Boyarsky, T. Fromenteze, L. Pulido-Mancera, T. Sleasman, and D. R. Smith, Review of metasurface antennas for computational microwave imaging, IEEE. Trans. Antennas Propag. **68**, 1860 (2020).

[15] W. J. Padilla and R. D. Averitt, Imaging with metamaterials, Nat. Rev. Phys. **4**, 85 (2022).

[16] C. Saigre-Tardif, R. Faqiri, H. Zhao, L. Li, and P. del Hougne, Intelligent meta-imagers: From compressed to learned sensing, Appl. Phys. Rev. **9**, 011314 (2022).

[17] S. M. Popoff, G. Lerosey, R. Carminati, M. Fink, A. C. Boccara, and S. Gigan, Measuring the transmission matrix in optics: an approach to the study and control of light propagation in disordered media, Phys. Rev. Lett. **104**, 100601 (2010).

[18] A. P. Mosk, A. Lagendijk, G. Lerosey, and M. Fink, Controlling waves in space and time for imaging and focusing in complex media, Nat. Photonics **6**, 283 (2012).

[19] N. Kaina, M. Dupré, M. Fink, and G. Lerosey, Hybridized resonances to design tunable binary phase metasurface unit cells, Opt. Express **22**, 18881 (2014).

[20] Q. He, S. Sun, and L. Zhou, Tunable/reconfigurable metasurfaces: Physics and applications, Research (2019).

[21] R. J. Beneck, A. Das, G. Mackertich-Sengerdy, R. J. Chaky, Y. Wu, S. Soltani, and D. Werner, Reconfigurable antennas: A review of recent progress and future prospects for next generation, Prog. Electromagn. Res. **171**, 89 (2021).

[22] V. G. Ataloglou, S. Taravati, and G. V. Eleftheriades, Metasurfaces: Physics and applications in wireless communications, Natl. Sci. Rev. **10**, nwad164 (2023).

[23] A. I. Dimitriadis, N. V. Kantartzis, T. D. Tsiboukis, and C. Hafner, Generalized non-local surface susceptibility model and Fresnel coefficients for the characterization of periodic metafilms with bianisotropic scatterers, J. Comput. Phys. **281**, 251 (2015).

[24] A. Rahimzadegan, T. D. Karamanos, R. Alaee, A. G. Lamprianidis, D. Beutel, R. W. Boyd, and C. Rockstuhl, A comprehensive multipolar theory for periodic metasurfaces, Adv. Opt. Mater. **10**, 2102059 (2022).

[25] S. Abeywickrama, R. Zhang, Q. Wu, and C. Yuen, Intelligent reflecting surface: Practical phase shift model and beamforming optimization, IEEE Trans. Commun. **68**, 5849 (2020).

[26] R. J. Williams, E. De Carvalho, and T. L. Marzetta, in *2020 IEEE International Conference on Communications Workshops (ICC Workshops)* (IEEE, 2020), p. 1.

[27] F. H. Danufane, M. Di Renzo, J. De Rosny, and S. Tretyakov, On the path-loss of reconfigurable intelligent surfaces: An approach based on green's theorem applied to vector fields, IEEE Trans. Commun. **69**, 5573 (2021).

[28] M. Di Renzo, F. H. Danufane, and S. Tretyakov, Communication models for reconfigurable intelligent surfaces: From surface electromagnetics to wireless networks optimization, Proc. IEEE **110**, 1164 (2022).

[29] S. Molesky, Z. Lin, A. Y. Piggott, W. Jin, J. Vucković, and A. W. Rodriguez, Inverse design in nanophotonics, Nat. Photonics **12**, 659 (2018).

[30] R. E. Christiansen and O. Sigmund, Inverse design in photonics by topology optimization: Tutorial, JOSA B **38**, 496 (2021).

[31] Z. Li, R. Pestourie, Z. Lin, S. G. Johnson, and F. Capasso, Empowering metasurfaces with inverse design: principles and applications, ACS Photonics **9**, 2178 (2022).

[32] A. M. Hammond, A. Oskooi, M. Chen, Z. Lin, S. G. Johnson, and S. E. Ralph, High-performance hybrid time/frequency-domain topology optimization for large-scale photonics inverse design, Opt. Express **30**, 4467 (2022).

[33] M. P. Bendsoe and O. Sigmund, *Topology Optimization: Theory, Methods, and Applications* (Springer Science & Business Media, Heidelberg, 2013).

[34] Y. Augenstein and C. Rockstuhl, Inverse design of nanophotonic devices with structural integrity, ACS Photonics **7**, 2190 (2020).

[35] A. Y. Piggott, J. Lu, K. G. Lagoudakis, J. Petykiewicz, T. M. Babinec, and J. Vučković, Inverse design and demonstration of a compact and broadband on-chip wavelength demultiplexer, Nat. Photonics **9**, 374 (2015).

[36] L. Su, A. Y. Piggott, N. V. Sapra, J. Petykiewicz, and J. Vuckovic, Inverse design and demonstration of a compact on-chip narrowband three-channel wavelength demultiplexer, Acs Photonics **5**, 301 (2018).

[37] R. Pestourie, C. Pérez-Arancibia, Z. Lin, W. Shin, F. Capasso, and S. G. Johnson, Inverse design of large-area metasurfaces, Opt. Express **26**, 33732 (2018).

[38] Z. Lin and S. G. Johnson, Overlapping domains for topology optimization of large-area metasurfaces, Opt. Express **27**, 32445 (2019).

[39] Y. Augenstein, A. Vetter, B. V. Lahijani, H. P. Herzig, C. Rockstuhl, and M.-S. Kim, Inverse photonic design of functional elements that focus Bloch surface waves, Light Sci. Appl. **7**, 104 (2018).

[40] Y. Augenstein, M. Roussey, T. Grosjean, E. Descrovi, and C. Rockstuhl, Inverse design of cavities for Bloch surface waves interfaced to integrated waveguides, Photonics Nanostructures: Fundam. Appl. **52**, 101079 (2022).

[41] D. E. Goldberg, *Genetic Algorithms in Search, Optimization & Machine Learning* (Addison-Wesley, 1989).

[42] N. Aage, E. Andreassen, B. S. Lazarov, and O. Sigmund, Giga-voxel computational morphogenesis for structural design, Nature **550**, 84 (2017).

[43] O. Sigmund, On the usefulness of non-gradient approaches in topology optimization, Struct. Multidiscipl. Optim. **43**, 589 (2011).
[44] A. L. Moustakas, H. U. Baranger, L. Balents, A. M. Sengupta, and S. H. Simon, Communication through a diffusive medium: Coherence and capacity, Science **287**, 287 (2000).
[45] J. D. Jackson, *Classical Electrodynamics* (John Wiley & Sons Inc., New York, 1999), 3rd ed.
[46] S. G. Johnson, *Notes on adjoint methods for 18.335* (Introduction to Numerical Methods, 2012).
[47] A. Luce, R. Alaee, F. Knorr, and F. Marquardt, Merging automatic differentiation and the adjoint method for photonic inverse design, arXiv:2309.16731.
[48] R. Remmert, *Theory of Complex Functions* (Springer Science & Business Media, New York, 1991), Vol. 122.
[49] See Supplemental Material at http://link.aps.org/supplemental/10.1103/PhysRevApplied.21.044022 for the application of the adjoint method in Sec. II, the phase-set solutions for the examples in Sec. III, and the application of the method of images for the 2D cavity-antenna problem in Sec. III C.
[50] TheMathWorksInc., Optimization Zoolbox version: 9.2 (r2021b), 2021. https://www.mathworks.com.
[51] K. Schittkowski, Nlpql: A fortran subroutine solving constrained nonlinear programming problems, Ann. Oper. Res. **5**, 485 (1986).
[52] J. Nocedal and S. J. Wright, *Numerical Optimization* (Springer, New York, 1999).
[53] R. Faqiri, C. Saigre-Tardif, G. C. Alexandropoulos, N. Shlezinger, M. F. Imani, and P. Del Hougne, PhysFad: Physics-based end-to-end channel modeling of RIS-parametrized environments with adjustable fading, IEEE Trans. Wirel. Commun. **22**, 580 (2022).
[54] M. Lax, Multiple scattering of waves. II. The effective field in dense systems, Phys. Rev. **85**, 621 (1952).
[55] COMSOL Multiphysics v. 5.5., 2020. www.comsol.com.
[56] J. L. Volakis and K. Sertel, *Integral Equation Methods for Electromagnetics* (IET, 2012), Vol. 12.
[57] F. Lemoult, G. Lerosey, J. de Rosny, and M. Fink, Manipulating spatiotemporal degrees of freedom of waves in random media, Phys. Rev. Lett. **103**, 173902 (2009).
[58] A. Epstein, J. P. Wong, and G. V. Eleftheriades, Cavity-excited Huygens' metasurface antennas for near-unity aperture illumination efficiency from arbitrarily large apertures, Nat. Commun. **7**, 10360 (2016).
[59] J.-B. Gros, P. del Hougne, and G. Lerosey, Tuning a regular cavity to wave chaos with metasurface-reconfigurable walls, Phys. Rev. A **101**, 061801 (2020).
[60] E. Hecht, *Optics* (Addison Wesley, San Francisco, 2002), 4th ed.